Intelligent Computing
A SCIENCE PARTNER JOURNAL

RESEARCH ARTICLE

Information Transfer in Neuronal Circuits: From Biological Neurons to Neuromorphic Electronics

Daniela Gandolfi[1*], Lorenzo Benatti[2], Tommaso Zanotti[2], Giulia M. Boiani[1], Albertino Bigiani[1,3], Francesco M. Puglisi[2,3*], and Jonathan Mapelli[1,3*]

[1]Department of Biomedical, Metabolic and Neural Sciences, University of Modena and Reggio Emilia, Modena, Italy. [2]Department of Engineering "Enzo Ferrari", University of Modena and Reggio Emilia, Modena, Italy. [3]Center for Neuroscience and Neurotechnology, University of Modena and Reggio Emilia, Modena, Italy.

*Address correspondence to: daniela.gandolfi@unimore.it (D.G.); francescomaria.puglisi@unimore.it (F.M.P.); jonathan.mapelli@unimore.it (J.M.)

Citation: Gandolfi D, Benatti L, Zanotti T, Boiani GM, Bigiani A, Puglisi FM, Mapelli J. Information Transfer in Neuronal Circuits: From Biological Neurons to Neuromorphic Electronics. *Intell. Comput.* 2024;3:Article 0059. https://doi.org/10.34133/icomputing.0059

Submitted 15 September 2023
Accepted 13 December 2023
Published 1 February 2024

The advent of neuromorphic electronics is increasingly revolutionizing the concept of computation. In the last decade, several studies have shown how materials, architectures, and neuromorphic devices can be leveraged to achieve brain-like computation with limited power consumption and high energy efficiency. Neuromorphic systems have been mainly conceived to support spiking neural networks that embed bioinspired plasticity rules such as spike time-dependent plasticity to potentially support both unsupervised and supervised learning. Despite substantial progress in the field, the information transfer capabilities of biological circuits have not yet been achieved. More importantly, demonstrations of the actual performance of neuromorphic systems in this context have never been presented. In this paper, we report similarities between biological, simulated, and artificially reconstructed microcircuits in terms of information transfer from a computational perspective. Specifically, we extensively analyzed the mutual information transfer at the synapse between mossy fibers and granule cells by measuring the relationship between pre- and post-synaptic variability. We extended this analysis to memristor synapses that embed rate-based learning rules, thus providing quantitative validation for neuromorphic hardware and demonstrating the reliability of brain-inspired applications.

Introduction

The information transfer within neuronal circuits is a complex and nonlinear process involving the elaboration of analog signals, resulting in electroresponsiveness [1–3]. This activity relies on the time-dependent properties of release probability [4,5], neurotransmitter diffusion [6,7], receptor activation [8], and, finally, membrane potential integration kinetics [9,10]. Nevertheless, in an abstraction exercise, neurons can be conceptualized as digital devices conveying trains of bits, namely, action potentials or spikes, whose transmission dynamics can be altered by the expression of activity-dependent changes in synaptic strength [11,12]. This reductionist perspective is essential when attempting to quantify the information transfer in neuronal circuits and, more importantly, when integrating biological dynamics into neuromorphic hardware [13,14]. The language employed by neurons to communicate can be analyzed by adopting parameters taken directly from information and communication theory and calculating mutual information (MI). MI serves as a quantitative measure of the amount of information transmitted by synapses and single neurons within neuronal populations. It is derived directly from variability in response to the same or separate inputs and provides a method for estimating the capability of a neuronal circuit to distinguish inputs and thus to convey information [15,16]. In this context, it is important to note that although several neuronal circuits adopt rate-based coding to communicate [17], as in the case of oscillatory activity detected in sensory [18] and motor neurons [19], information can also be transferred through synchronization and spike time coincidence [20], thus playing a crucial role in the induction of several forms of long-term plasticity [21]. Interestingly, the majority of neuromorphic applications lay their foundations in firing rate coding [22], leaving potential applications based on time coding largely unexplored.

In this context, neuromorphic technologies have been designed and developed to support the simulation of neuronal networks based on spike transfer through synaptic contacts, incorporating bio-inspired mechanisms. It has been shown that the memristor, the electronic equivalent of a biological synapse, can reliably reproduce one of the most salient features of the latter, i.e., long-term plasticity [23,24]. Notably, although several neuromorphic architectures have been proposed to embed the learning rules required to fully instantiate neuronal network functionality, a clear demonstration of the effective capabilities of electronic systems to replicate the information transfer typical of biological systems is yet to be achieved.

The estimation of information transfer can be performed by quantifying the amount of information conveyed by neural responses in relation to input stimuli [25–28], treating neurons as stochastic communication channels. According to information theory, it is possible to estimate the amount of information transmitted by a neuron in different contexts, such as sensory stimulation [29,30] or adaptation in visual receptive fields [31]. At the subcellular level, the efficiency of information transfer in single synapses has been measured using information theory [27,32–34]. Given that MI provides a correlation between input stimuli and neuron responses, and that its estimate can be assessed by determining the probability distribution of output spikes given any input, the main limitation of MI calculation is therefore the size of the input/output (I/O) space [26]. A typical biological neuron receives thousands of synaptic contacts from different neurons across its dendritic tree, tremendously expanding the size of the I/O space. The cerebellar circuit [35,36], particularly the input stage, provides an optimal framework for overcoming this issue by virtue of a series of factors: (a) the granule cells (GrCs) are small neurons (on average ~6 μm in diameter) receiving a limited number of excitatory inputs (4.38 on average; [37]); (b) their membrane potential is stable, and intrinsic firing is absent [7,38]; (c) they show stereotyped response patterns with a limited number of spikes (less than two) confined in a narrow time window that has been well characterized [39]; (d) the synapse between mossy fiber (MF) and the GrCs relies on glutamatergic transmission, which is controlled by both pre- and post-synaptic mechanisms that have been thoroughly characterized. Most importantly, a complete computational model of the microcircuit has been validated and repeatedly employed in various contexts [39–41].

From a broader perspective, artificial intelligence (AI) applications rely on learning algorithms that in some cases have shown performance surpassing human levels in various types of individual tasks [42]. Nevertheless, human intelligence performs unlimited tasks by continually learning and accumulating knowledge, exceeding the capabilities of modern deep learning methods with incomparable superiority. Furthermore, the limited energy efficiency of modern AI systems necessitates alternative approaches that can address the forthcoming challenges facing our society. Among these alternatives, spiking neural networks (SNNs), which rely on parallelized and desynchronized computational architectures, represent a promising neuro-inspired method to achieve human brain performance. Unfortunately, despite efforts in developing SNNs, the performance gap with traditional artificial neural network (ANN)-based AI systems has yet to be completely bridged. Recently, compelling results in the field of SNNs have been achieved by algorithms capable of performing continual meta-learning based on minimum error entropy [43], few-shot online learning through a combination of recurrent network architecture and entropy theory [44], and fault-tolerant edge computing for navigation tasks through the implementation of a neuromorphic dopaminergic circuit [45]. SNNs serve as a theoretical and computational foundation for realizing neuromorphic computing platforms supported by robust and efficient neuromorphic electronics. This aspect is particularly relevant because the development of innovative bio-inspired devices such as memristors and synaptic transistors [46] is expected to greatly affect data storage and, more importantly, computing methodologies. This would allow artificial circuits to perform bioinspired operations such as dendritic computations [47] and play a critical role in functions like spatial navigation and sensory processing. The mimicry of neural functions in hardware has the potential to enable high-performance superparallel in-memory computing and thus overcome the von Neumann bottleneck. In this regard, neuromorphic hardware platforms can benefit from the co-location of memory and processing features because synaptic devices (e.g., memristors) can perform nonvolatile computation and show responses to spike stimuli that resemble those experimentally detected in biological computation and learning patterns. Importantly, these features eliminate the continuous, slow, and energy-intensive shuttling of data between memory and the central processing unit that is required by conventional computing architectures. It is this data shuttling that is largely responsible for the substantial energy inefficiency of state-of-the-art AI systems and hinders their integration into portable devices and impedes the advent of the era of pervasive and ubiquitous AI.

The conversion of biological circuits into neuromorphic electronics requires consideration of all these aspects. In this study, we begin by quantifying information transfer in different biological and artificial systems. We compare the information transfer of experimental, computational, and electronic models of cerebellar microcircuits, with a specific focus on the impact of long-term synaptic plasticity on MI values. It is known that the expression of long-term potentiation (LTP) and long-term depression (LTD) alters communication channels within neuronal networks [48,49], although a quantitative demonstration is still lacking. Since the mechanisms underlying the induction and expression of long-term synaptic plasticity at the MF to GrC synapse have been thoroughly studied, such a synapse represents an ideal standard to be adopted in the present investigation. Furthermore, most of these mechanisms rely on presynaptic changes that are traceable to release probability modulation; therefore, they can be simulated in software [15] and reproduced in hardware. Given that much of the effort in the neuromorphic community has been dedicated to the design, development, and implementation of electronic solutions that mimic learning rules rather than to quantifying the computational performance of the hardware, we have tested the biological soundness of an artificial network from the perspective of information transfer. This represents a key step toward brain-inspired low-power artificial systems.

Materials and methods

Experiments were conducted using Sprague-Dawley rats at postnatal days P17 to P24 [Charles-Rivers (Calco, Lecco, Italy) and internal breeding]. All experiments were conducted in accordance with international guidelines outlined in the European Community Council Directive 86/609/EEC regarding the ethical use of animals. Approval for the experiments was obtained from both the Ethical committee of the Italian Ministry of Health and the Ethical Committee of the University of Modena and Reggio Emilia. Furthermore, the study was performed in compliance with the ARRIVE guidelines (https://arriveguidelines.org/). Animals ($n = 4$) were selected without consideration of gender, and a total number of 16 cells were employed to perform this research.

Recordings in acute cerebellar slices

Patch-clamp recordings were obtained from parasagittal cerebellar slices, following previously established procedures [50]. Briefly, rats were anesthetized with isoflurane (Sigma-Aldrich, St. Louis, MO, USA) and decapitated. After removal, the cerebellar vermis was isolated and fixed using cyanoacrylic glue on a vibroslicer stage (VT1000S, Leica Microsystems, Nussloch, Germany). Acute thick slices (200 µm) were cut in a cold cutting solution containing 130 mM K-gluconate, 15 mM KCl, 0.2 mM EGTA, 20 mM HEPES, and 10 mM glucose (pH adjusted to 7.4 with NaOH). Slices were incubated in oxygenated extracellular Krebs solution containing 120 mM NaCl, 2 mM KCl, 1.2 mM $MgSO_4$, 26 mM $NaHCO_3$, 1.2 mM KH_2PO_4, 2 mM $CaCl_2$, and 11 mM glucose (pH 7.4 when equilibrated with 95% O_2 and 5% CO_2) at 32 °C for at least 1 hour before recordings. Subsequently, slices were transferred to a recording chamber on the stage of an upright microscope (Zeiss Axioexaminer A1, Oberkochen, Germany), immobilized with a nylon mesh attached to a platinum Ω-wire, and perfused at 1.5 ml min^{-1} with the same oxygenated Krebs solution, maintained at 32 °C with a thermostatic controller (Multichannel systems GmbH, Reuntlingen, Germany).

Intracellular recordings were performed in a whole-cell patch-clamp configuration, following previously established procedures [39], from GrCs preferentially selected in the central lobules of the vermis (from IV to VII). Recordings were obtained using an Axopatch 200 B amplifier (Molecular Devices, Union City, CA, USA) (−3 dB; cutoff frequency = 2 kHz) and digitized at 20 kHz using pClamp 9 (Molecular Devices) and a Digidata 1322A A/D converter (Molecular Devices). Patch pipettes were made with a vertical puller (model PP-830, Narishige, Tokyo, Japan) from borosilicate glass capillaries and filled with the following intracellular solution: 126 mM K-gluconate, 8 mM NaCl, 15 mM glucose, 5 mM HEPES, 1 mM $MgSO_4$, 0.1 mM BAPTA-free, 0.05 mM BAPTA-Ca^{2+}, 3 mM adenosine triphosphate (ATP), and 100 µM guanosine triphosphate (GTP) (pH adjusted to 7.2 with KOH). This solution maintained resting-free $[Ca^{2+}]$ at 100 nM, and the pipettes had a resistance of 7 to 10 MΩ before seal formation. Passive cellular parameters were monitored at the beginning of every voltage-clamp recording session to assess the stability of the series resistance by measuring and analyzing the current relaxation induced by a 10-mV step from a holding potential of –70 mV. The transients were reliably fitted with monoexponential functions, resulting in a membrane capacitance (C_m) of 2.1 ± 0.5 pF ($n = 16$), a membrane resistance (R_m) of 2.0 ± 0.6 GΩ ($n = 16$), and a series resistance (R_s) of 16.8 ± 2.8 MΩ ($n = 16$), in close similarity with previous results [51]. Afferent MFs were stimulated through an isolated bipolar tungsten electrode (Clark Instruments, Pangbourne, UK) at a stimulation intensity of ±4 – 12 V (duration 100 µs). During stimulation, GrCs were maintained at a membrane potential between −70 and −60 mV (mean −64.1 ± 4.8 mV, $n = 16$). Under the same conditions, previous analyses [7,52] estimated the average number of stimulated fibers per GrC to be in the range from 1 to 3.

MI estimation

The amount of MI transferred and the relative changes due to the expression of long-term plasticity were calculated following the approach outlined in [15,16]. Briefly, information theory was used to correlate the input stimuli and output responses [53] by generating time windows (temporal bins) of neuronal responses digitized based on the presence of a spike (Fig. 1). The degree of correlation was assessed by measuring the response entropy (RE), a quantity representing the variability of responses to a specific set of input stimuli. According to Shannon's theory [54], the higher the RE, the better the system communicates. To account for systematic noise arising from the intrinsic noisiness of neuronal systems, noise entropy (NE) was introduced. The robustness of the system is quantified by subtracting NE from RE. MI, measured in bits, is calculated as follows:

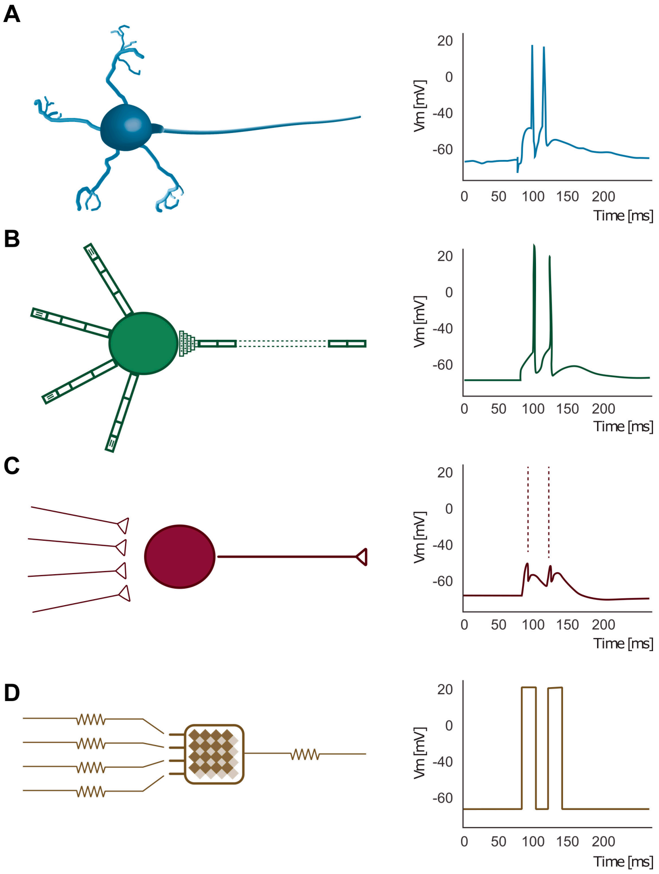

Fig. 1. Study design. (A) Left: Cerebellar granule cell (GrC) in its realistic morphological representation with four dendrites ending in characteristic claw-like spines. Right: Firing pattern recorded in a current clamp configuration from a GrC and evoked with a pair of stimuli at 50 Hz. (B) Left: Cerebellar GrC reconstructed with a morphologically detailed computational model. Each of the four dendrites has 4 compartments, whereas the axon hillock and the axon have a total of 37 compartments. Right: Firing pattern evoked with a pair of stimuli at 50 Hz in the simulated neuron shown on the left. (C and D) Similar to (A) and (B), the simulated and the electronic point neuron GrC have a single compartment and receive four inputs. The firing pattern evoked by a pair of stimuli at 50 Hz evoked two spikes.

$$MI = \sum_r \sum_s p(s)p(r|s)\log_2 \frac{p(r|s)}{p(r)}$$

where r and s are expressed in binary digits and represent the response and the stimulus patterns; $p(r)$ and $p(s)$ are the probabilities of occurrence in one acquisition of r and s, respectively; and $p(r|s)$ is the probability of having a specific r, given a specific s. The accuracy of the MI calculation increases with the accuracy of the probability estimation. As an increase in repetitions can limit the intrinsic variability of responses, we have employed a biologically plausible circuit that has been demonstrated to be suitable for MI estimations [16] in different conditions.

The MI estimation was computed by spike-sorting and digitizing the GrC responses (MATLAB; Mathworks Inc., Oregon, USA; Fig. 1C). With a 10-ms bin size and a 40-ms stimulus duration, the number of possible combinations (16) was reduced to 8 by discarding duplications (e.g., 1100, 0110, 1100, and 0011) and irrelevant patterns (0000). The limited input space accounted for the typical discharge patterns of the MF (two to four spikes at 100 Hz). Moreover, since the GrC firing frequency is approximately 150 Hz with less than five to six spikes [39], a 60-ms output time window with a 6-ms bin was adopted. Furthermore, response variability was reduced by repeating the same stimulus 25 times, even though the number of possible output combinations (210) was much higher. This approximation has been derived from [15], where a similar approach provided a good estimation, particularly for MI values larger than 0.4 bits.

The MI was decomposed into the single stimulus contribution [stimulus-specific surprise (*sss*)] and the single spike contribution [surprise per spike (*sps*)] and calculated using the following equations:

$$I\left(s^*\right) = sss \;=\; \sum_r \left(p|rs^*\right) \log_2 \frac{\left(p|rs^*\right)}{p(r)}$$

$$I_{perSpike}(s^*) = sps = \frac{I(s^*)}{stimulus\ spike\ count}$$

Surprise is a measure of the difference between the conditional distribution of $p(r|s)$ and the probability distribution $p(r)$. The surprise per spike was calculated by dividing the surprise by the spike count of the input stimulus.

Finally, neurotransmission and synaptic plasticity were quantified by calculating the following parameters: (a) spike probability (*sp*); (b) number of emitted spikes (*ns*); (c) average first spike delay (*sd*); (d) first spike jitter (*sj*), measured as the standard deviation of the first spike delay; and (e) firing frequency (*ff*), estimated as the average inverse of the interspike interval when measurable.

Long-term plasticity induction and analysis

Long-term plasticity was induced by delivering a theta-burst stimulation (TBS; 10 pulses at 100 Hz delivered eight times at 4 Hz) protocol in a current-clamp configuration from −60 mV. GrCs were monitored in voltage-clamp configurations (holding cells at −70 mV) to detect excitatory post-synaptic currents (EPSCs) evoked by paired stimulation at 50 Hz. Fifty consecutive responses were recorded, and EPSCs were averaged [29.7 ± 4.4 pA (n = 16) [40]]. Moreover, the paired pulse ratio (PPR) was calculated as the ratio between the first and second evoked EPSC of each repetition [0.78 ± 0.05 (n = 16) [52]]. Finally, excitatory post-synaptic potentials (EPSPs) evoked by individual stimuli were used to assess the stability of the recording sessions and the variations induced by TBS. The average EPSP amplitude was 11.4 ± 0.9mV (n = 16 cells).

Biologically realistic simulations (GrCHH)

Simulations of the microcircuit with a realistic multi-compartmental model of the neuron were performed using the NEURON simulator (v 8.9) and Python (v.3.8.8) and run on a personal computer with an AMD Ryzen 5 3600 6-core processor running at 3.60 GHz. The model was originally presented in [7] and modified and refined in [40,41]. It describes the functioning of the synapses of single neurons, accounting for vesicular dynamics, neurotransmitter spillover, and receptor gating (including multiple closed, desensitized, and open states), but not for quantal release mechanisms. It reliably reproduces the kinetics and size of the post-synaptic currents (axonal conduction times were considered negligible, and the transmission delay was set to 1 ms for all the synapses). The GrC model describes the morphological structure and the localization and dynamics of ion channels. The soma had a 5.8-μm diameter attached to four identical unbranched dendrites (15-μm diameter), subdivided into 4 compartments, and to the axon (0.75-μm diameter) with 5 proximal and 30 distal compartments. For each compartment, the Hodgkin–Huxley equation was solved, and the voltage was evaluated for each time step (where the time step was $dt = 0.025$ ms). The current was clamped to hold the resting potential at −65 mV.

Four identical independent synapses with distinct pre- and post-synaptic dynamics were used to create the synaptic model of GrCs. At the MF-GrC synapse, the short-term dynamics of the EPSCs were derived from the Tsodyks and Markram [55] three-state scheme accounting for synaptic facilitation and depression.

The microcircuit was constructed by connecting four MFs to a single GrC. The connection weights were randomly varied at each simulation trial, with each MF-GrC synapse being assigned a weight value selected from a distribution centered at 1 and with a standard deviation of 0.25. The stimulation pattern consisted of four inputs at 100 Hz that were switched on or off according to eight different combinations: [1,0,0,0], [1,1,0,0], [1,0,1,0], [1,0,0,1], [1,1,1,0], [1,1,0,1], [1,0,1,1], and [1,1,1,1]. All the stimuli simultaneously impinged on all the MFs.

Synaptic and neuronal devices

According to the configuration adopted in the biological experiments (Fig. 1) and simulations (Figs. 2 and 3), a cerebellar GrC-like artificial complementary metal-oxide-semiconductor (CMOS) neuron with four memristor-based synaptic inputs was implemented to investigate the changes in information transfer induced by long-term plasticity. The circuit simulations were run using Cadence Virtuoso software, as in [14]. Briefly, the responses of the artificial CMOS neuron were abstracted by using a Verilog-A behavioral description of its constituent building blocks, and the properties of the artificial synapses were reproduced using an in-house-developed compact model (the UniMORE RRAM Model [56]). The adopted memristive elements were commercially available C-doped self-directed channel (SDC) memristors [57] available in a dual in-line package (DIP). To the best of our knowledge, these are the only commercially available packaged resistive random access memory (RRAM) devices. Therefore, it was possible to demonstrate that MI propagates through an SNN with CMOS leaky integrate-and-fire (LIF) neurons and memristive synapses. More importantly, we demonstrated that no specific technological advancements are required to show this behavior. The SDC memristor consists of a stack composed of W/Ge_2Se_3/Ag/Ge_2Se_3/SnSe/Ge_2Se_3:C/W, where Ge_2Se_3:C is the active layer [57]. During device fabrication, the three active layers below the top electrode (TE) intermix to form an Ag ion source [57]. The SnSe layer acts as a barrier to prevent Ag saturation in the active Ge_2Se_3:C layer and is responsible for the production of Sn ions and their migration into the active Ge_2Se_3:C layer

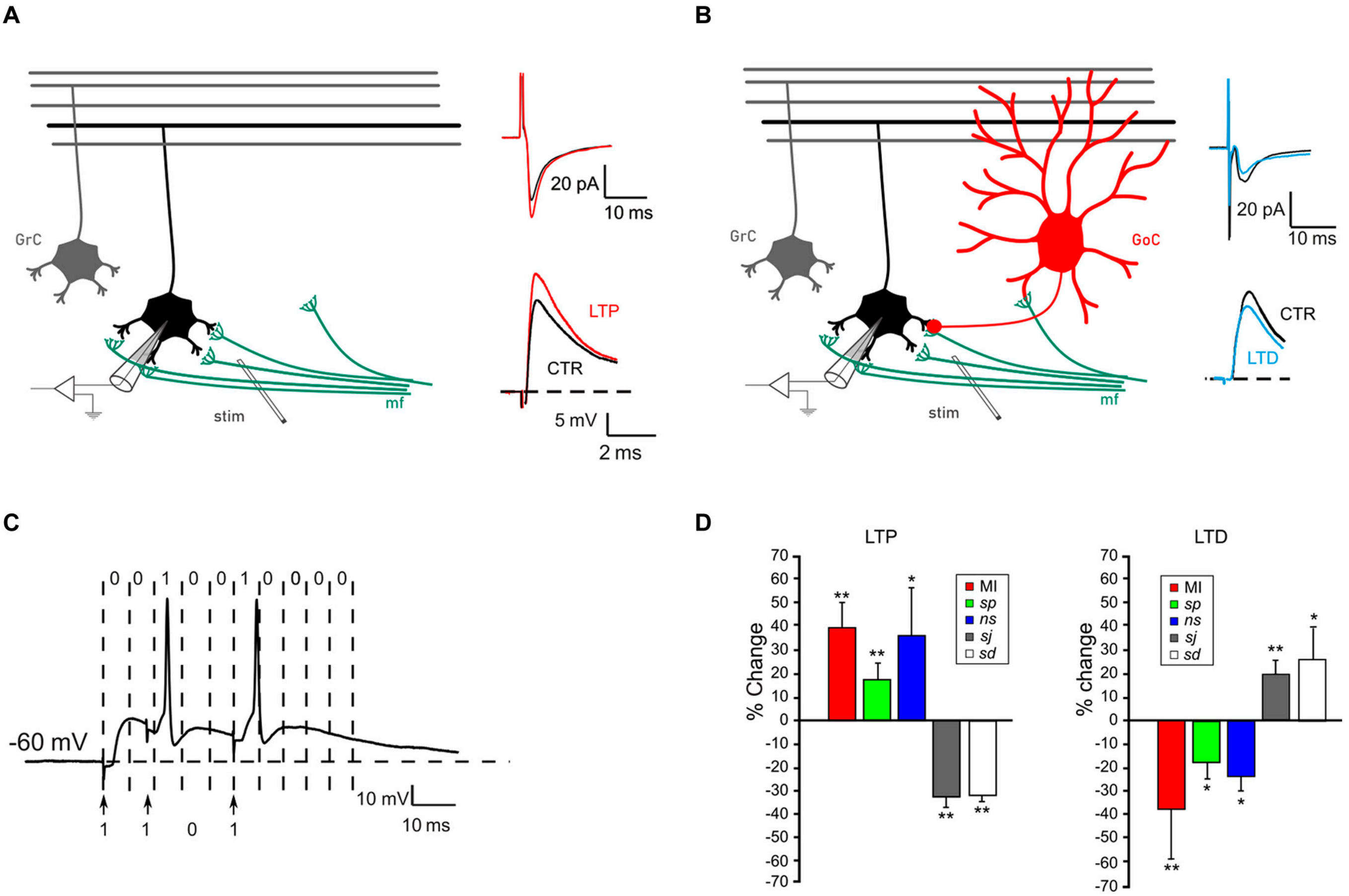

Fig. 2. MI changes upon the expression of long-term plasticity. (A) Left: Granular layer microcircuit with a stimulating electrode (stim) positioned onto the mossy fiber bundle (mf). The block of GABAergic inhibition allows only excitatory synapses to be activated. Right, top: Black trace represents the average of 10 synaptic responses obtained in voltage clamp configuration in control conditions (CTR). The red trace shows the average synaptic response obtained following the expression of LTP. Bottom: Similarly, voltage traces show the increase in the average response obtained following LTP induction in current clamp configuration. (B) The same circuit shown in (A) is now represented with the Golgi cell (GoC; a local interneuron, in red) inhibiting GrC responses. A configuration with active inhibition was adopted to preferentially induce LTD. Right, top: Black trace represents the average of 10 synaptic responses obtained in voltage clamp configuration in control conditions. The blue trace shows the average synaptic response obtained following the expression of LTD. Bottom: Similarly, voltage traces show the increase in the average response obtained following LTP induction in current clamp configuration. (C) Spike detection procedure generating binary digits. A single response of a GrC to three pulses at a variable frequency (code 1101, arrows). The spike in each 6-ms time window determines the output code in binary digits (0010010000, top). (D) Left: Effects induced by LTP on MI transfer (red, 39.6% ± 10.8%, $P < 0.001$) and spike-related parameters (*sp*, green, 17.8% ± 5.8%, $P < 0.001$; *ns*, blue 36.4% ± 19.3%, $P < 0.05$; *sj*, gray, −32.5% ± 5.1%, $P < 0.001$; *sd*, white, −31.6% ± 3.9%, $P < 0.001$; $n = 7$). Right: Effects induced by LTD on MI transfer (red, −37.5% ± 20.9%, $P < 0.01$) and spike-related parameters (*sp*, green, −18.7% ± 7.4%, $P < 0.05$; *ns*, blue −24.7% ± 10.3%, $P < 0.05$; *sj*, gray, 20.9% ± 7.3%, $P < 0.01$; *sd*, white, 29.8% ± 16.4%, $P < 0.05$; $n = 5$).

during the initial operation of the device (typically addressed as "forming"), thus promoting Ag agglomeration at specific sites. The details of the mechanism at the basis of the resistive switching in these devices are available in [57]. To correctly reproduce the behavior of SDC memristors in circuit simulations, a careful calibration of the UniMORE RRAM Model parameters was conducted using experimental data from electrical measurements performed using a Keithley 4200-SCS, as described in [24]. A first set of electrical measurements was aimed at verifying the baseline functionality of the device and consisted of a sequence of quasi-static current acquisitions by applying slow voltage sweeps in the −0.8-V to 0.4-V range, using a current compliance of 10 μA directly provided by the Keithley 4200-SCS. Such electrical stimuli force the device to switch between a low resistive state (LRS) using the SET operation ($V > 0$) and a high resistive state (HRS) using the RESET operation ($V < 0$). Subsequently, a second set of electrical measurements was conducted to evaluate the synaptic functionality of the memristors (i.e., their capability to respond to spike-like voltage stimuli rather than to quasi-static voltage sweeps) by applying a pulsed voltage sequence (i.e., a spike sequence), gradually driving the device resistance toward higher or lower values. The results confirmed a smooth and reproducible synaptic analog behavior, with LTD and LTP achieved by applying trains of 20 depression pulses ($V = -0.2$ V, $T = 10$ μs) followed by 20 potentiation pulses ($V = 0.55$ V, $T = 30$ μs). Each potentiation or depression pulse was succeeded by a small reading pulse ($V_{\mathrm{READ}} = 50$ mV, $T_{\mathrm{READ}} = 50$ μs) to retrieve the evolution of the resistance values during LTD and LTP.

SDC memristors are ion-conducting memristive devices that modulate their resistance because of the motion of Ag^+ ions within the device. Nonetheless, their behavior is well captured by the UniMORE RRAM Model because it can be equally well described in terms of the equivalent modulation of the thickness of a dielectric barrier within a conducting filament. This latter behavior is typical of the filamentary memristive

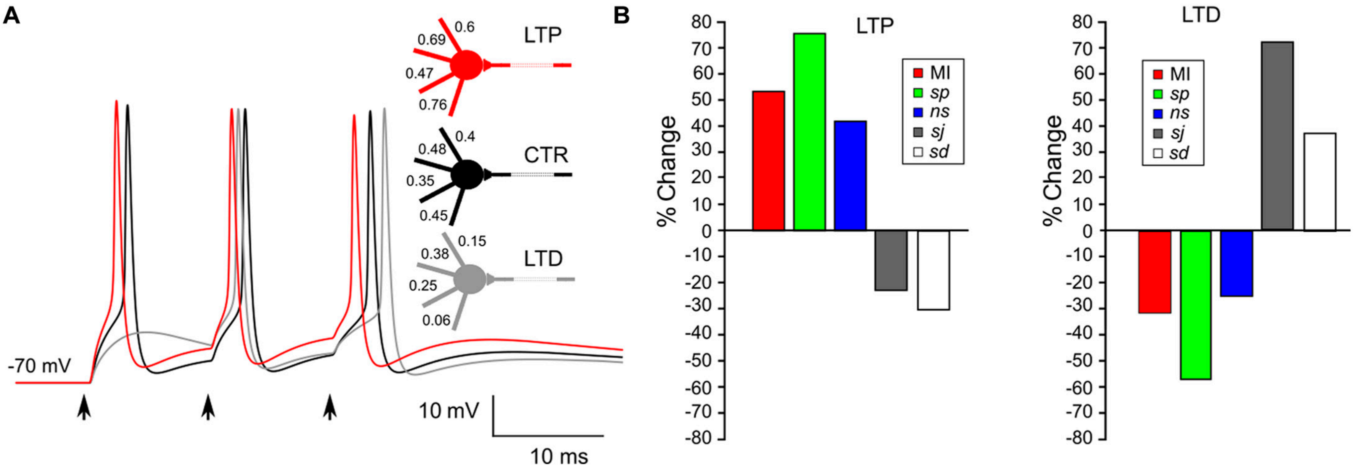

Fig. 3. MI changes in GrCHH. (A) Firing pattern of the simulated GrCHH neuron model in response to three inputs delivered at 100 Hz under different simulated conditions (CTR, control black trace; LTP, red trace; LTD, gray trace). The numbers next to each dendrite represent the random distribution of release probability during the stimulation. (B) Changes in MI and spike-related parameters following LTP (left) and LTD (right).

devices for which the UniMORE RRAM Model was originally conceived. The barrier thickness is directly related to the memristor conductance, which, in turn, is representative of the synaptic strength. The details of the experiments and the ensuing UniMORE RRAM Model parameter calibration are provided in [24].

Results and Discussion

We analyzed the changes in MI transfer following the expression of long-term plasticity in a real microcircuit, in various simulated environments, and in an electronic neuromorphic system (Fig. 1).

Biological neurons

We began by assessing changes in MI transfer in the cerebellar input stage microcircuit by performing whole-cell patch-clamp recordings from cerebellar GrCs. Current-clamp recordings of these neurons were performed while eliciting excitatory synaptic activation through repetitive MF stimulation (Fig. 2). Spike detection was arranged in such a way as to generate binary digits, representing sequences of the GrC output to input patterns (see Materials and Methods for a complete description of the MI calculation; see also [16]). MI was estimated as a combination of spike number, precision, and probability of firing by presenting eight types of stimulation patterns resulting from all possible MF input combinations (see Materials and Methods). In line with prior experimental findings, the calculation of MF-GrC MI transfer revealed a value of 2.45 ± 0.41 ($n = 9$), showing a basal level of functional correlation between the input signals and GrC responses that was slightly larger than that previously recorded for the same circuit [15,16]. This could be due to the presence of the $\mathrm{GABA_A}$ receptor blocker gabazine in the bath solution. Gabazine increases GrC firing activity and, therefore, increases the probability of inducing LTP during the TBS protocol (Fig. 2A). Indeed, in response to TBS, the majority of GrCs (seven out of nine) improved their synaptic responses based on LTP expression [51,58]. Conversely, one cell that underwent LTD exhibited decreased synaptic responses, whereas the remaining cells showed no discernible changes (Fig. 2B). In line with the changes induced by LTP in GrCs firing (firing probability $sp = +17.8\% \pm 6.8\%$; total number of emitted spikes $ns = +36.4\% \pm 20.3\%$; spike jitter $sj = -32.5\% \pm 5.1\%$; first spike delay $sd = -31.6\% \pm 3.9\%$; $n = 7$; Fig. 2D), cells undergoing LTP showed an increase in MI transfer (39.6% ± 10.8%; $n = 7$; Fig. 2C and D), consistent with previous observations and theoretical predictions. The induction of LTD was performed by maintaining GABAergic inhibition through Golgi cell activity [50,59]. In this experimental configuration, the MI transfer was compatible with previous observations (1.9 ± 0.35; $n = 5$) and, in response to the expression of LTD, the MI transfer markedly decreased (−49.2% ± 24.3; $n = 5$). The down-regulation of MI induced by LTD was associated with changes in firing parameters, as in the case of synaptic potentiation but with opposite signs (Fig. 2D).

Simulated neurons

Modeling neuronal activity is a challenging undertaking due to the large number of characteristics that must be considered when reproducing a complex system, such as a neuron and its connections [60,61]. The level of biological detail reproduced by the model affects the realism of the simulation, and the required computational capacity scales up with the size of the simulated circuit [62,63]. The most detailed class of computational models of neuronal electrical behavior is the Hodgkin and Huxley model (HH-model; [64]). Models of this class are typically constructed according to the morphological characteristics of single neurons and are implemented with a variable number of dendritic and axonal compartments that have specific structural properties and are equipped with ionic channels distributed according to experimental data. A biologically realistic model of the cerebellar GrC [7] has been employed to explore the impact of LTP and LTD on information transfer (GrCHH; Fig. 3A). Similar to what has been shown in [15,16], the granule cell Hodgkin and Huxley model (GrCHH) has been connected to excitatory MFs via AMPA (α-amino-3-hydroxy-5-methyl-4-isoxazolepropionic acid) and NMDA (*N*-methyl-D-aspartate) glutamatergic synapses, which were stimulated with the same stimulation patterns adopted in the experiments. Changes in synaptic weights have been simulated by increasing or decreasing the release probability since both LTP and LTD at the MF-GrC synapse are mainly expressed as presynaptic mechanisms [65]. As expected, simulating an increase in the release probability resulted in increases in the total number of emitted spikes (+45.1%) and in the firing probability (+75.5%) coupled with decreases in first-spike delay (−29.6%) and variability (−20.3%). Conversely, the decrease in release probability induced a delayed first spike (39.6%) with an increased variability (+73.9%) and decreased the total number of emitted spikes (−57.8%) and the firing probability (−77.8%). As a whole, these changes in synaptic behaviors influenced the MI transfer, which increased upon LTP (from 3.01 with $P = 0.42$ to 4.6 with $P = 0.63$; +53.7%) and decreased following LTD (from 3.01 with $P = 0.42$ to 2.01 with $P = 0.21$; −33.2%; Fig. 3B).

From the perspective of translating biological neurons into neuromorphic circuits, we have also tested the MI transfer using a simplified version of a neuronal model. The conversion of the HH model into an electronic architecture has been recently proposed [66]. However, the number of parameters that must be tuned to describe the action potential dynamics in a single neuron severely limits the hardware implementation of large-scale networks. In most cases, this limitation has led to the use of simplified neuron implementations such as the integrate-and-fire (IAF) model. In this case, the membrane potential value is calculated numerically during synaptic integration, and after overcoming the spike threshold, it is forced to return to its resting value without spending time on further computation. Following the GrCHH model, the granule cell integrate-and-fire model (GrCIAF; Fig. 4A) was connected to four excitatory inputs, and the stimulation patterns were delivered to quantify the MI transfer. Changes in synaptic release simulating the expression of presynaptic LTP and LTD were mimicked by varying the weights of AMPA and NMDA. The synaptic parameters activating the IAF neuron connected to the excitatory inputs were calibrated to generate response patterns compatible with the experimental results (Fig. 4). Analogous to the biologically detailed model, simulating LTP increased firing activity (*fp* +70.8%; *ns* +54%; Fig. 4B) and reduced first spike variability and delay (*sj* −23.6%; *sd* −28.2%; Fig. 4B). Conversely, simulating the expression of LTD resulted in decreased firing activity (*fp* −48.1%; *ns* −55%; Fig. 4B), coupled with increased first-spike variability and delay (*sj* +22.7%; *sd* +58.8%; Fig. 4B). Accordingly, the MI transfer increased from 1.64 to 2.52 (+53.7%; Fig. 4B) upon the increase of synaptic weights, whereas it decreased to 0.33 in response to LTD (−79.9%; Fig. 4B). These results show that despite assumptions leading to an overall reduction in the complexity of molecular and cellular behavior, models that treat neuronal activity as a single-point element are a reliable tool for evaluating how neuronal circuits transmit information and can be faithfully translated into neuromorphic hardware.

Electronic neurons

As described in [14], a CMOS LIF neuron supporting a rate-dependent plasticity rule on memristive devices was designed and simulated to investigate changes in MI transfer. In this configuration, the input terminal integrates spikes from presynaptic neurons using a capacitor, included in the “integration box” shown in Fig. 5A. When the voltage exceeds a given threshold value (V_{TH}), an action potential is generated at the output. This is achieved by comparing the output of the integrator with that of the V_{TH} using a standard comparator based on an operational amplifier. The initial state of the integrator is restored by discharging the capacitor after a predefined delay. This is achieved by the T_{Spike} Delay block in Fig. 5A, which generates a logical “Reset” signal. This signal, in turn, temporarily influences the integrator (as symbolized by the dashed line connecting the input of the integrator to the ground). The presence of a reset-set latch allows for the triggering of the output “Spike” signal for a duration dictated by the T_{Spike} Delay block. This signal drives the waveform generator, which is designed to produce the correct output spike waveform at the “Neuron Out” terminal. Biological constraints are imposed by setting a dependency of the charging rate of the capacitor on both the input spike rate and the synaptic strength. Synaptic plasticity has been mimicked by translating the rate of presynaptic stimulation into the potentiation or depression of the corresponding synapse (Fig. 5A), which, in turn, is expressed as a relative change of the conductance ($\Delta G/G$; Fig. 5A). Specifically, the synaptic element (i.e., the memristor) was fed a specific potentiation or depression spike via access transistors, as illustrated

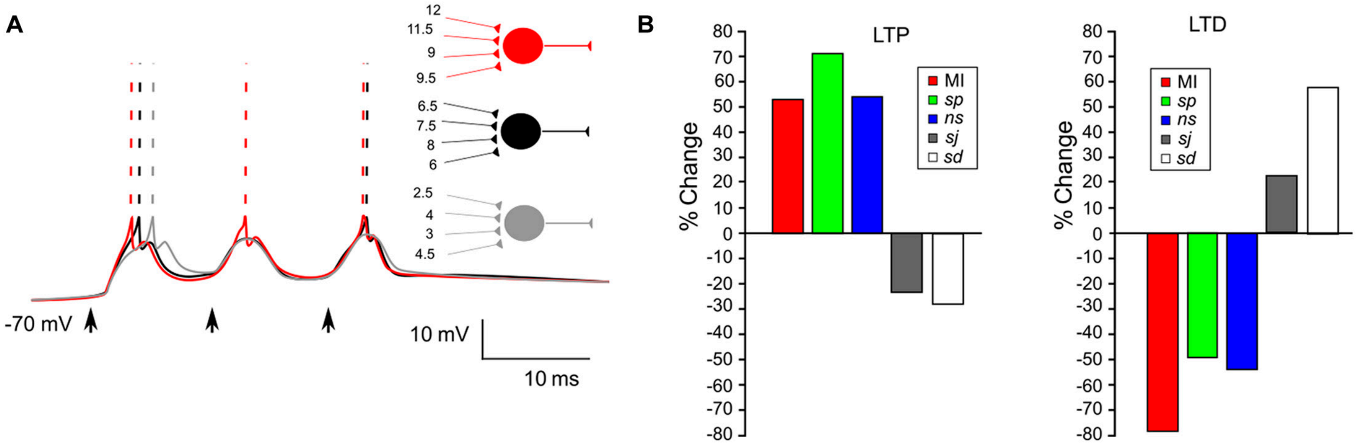

Fig. 4. MI changes in GrCIAF. (A) Firing pattern of the simulated GrCIAF neuron model to three inputs delivered at 100 Hz in different simulated conditions (control, black trace; LTP, red trace; LTD, gray trace). The numbers beside each dendrite represent the random distribution of synaptic weights during the stimulation. (B) Changes in MI and spike-related parameters following LTP (left) and LTD (right).

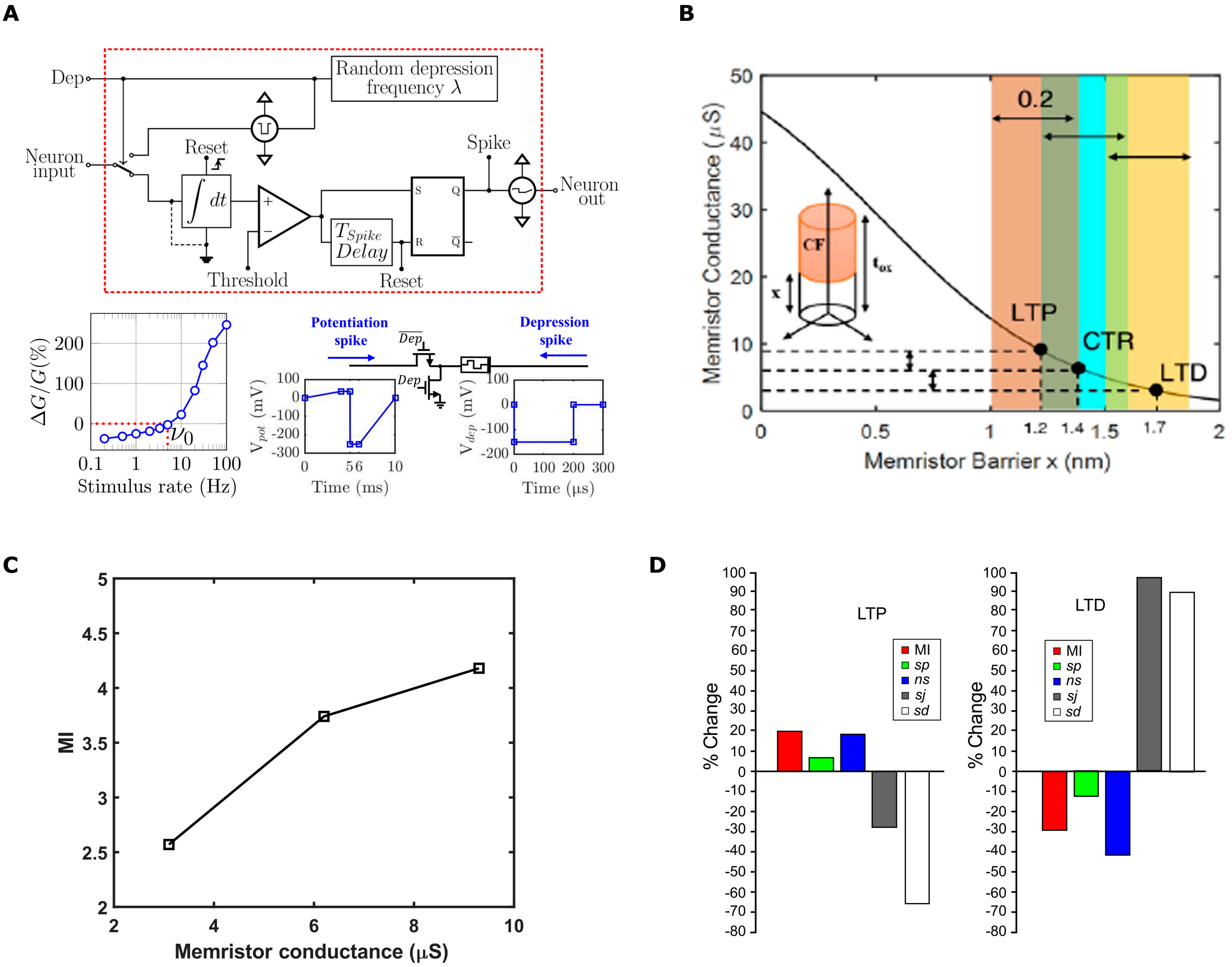

Fig. 5. Neuromorphic hardware. (A) Top: Schematic of the implemented LIF neuron. Bottom left: Synaptic plasticity is reproduced by a rate-based learning rule, with potentiation (depression) induced by a presynaptic stimulation rate higher (lower) than the threshold V_0. Bottom right: Shapes of the potentiation and depression spikes and their connections to the memristor. (B) Memristor conductance versus barrier (x) relation, derived from the UniMORE RRAM model. Each memristor condition (i.e., CTR, LTD, and LTP) is confined to $x \pm 0.2$ nm, with $x = 1.4$ nm for CTR, $x = 1.2$ nm for LTP, and $x = 1.7$ nm for LTD. (C) MI calculated for CTR, LTD, and LTP. The conductance values are 6, 3, and 9 μS, respectively, as evaluated from (B). (D) Effects induced by LTP (left) and LTD (right) on MI transfer and spike-related parameters.

in Fig. 5A (central panel, bottom line), to realize the corresponding operation. The shape of the spike was determined according to the specifications of the selected memristor technology.

The electronic GrC (eGrC) was simulated by employing spikes with a longer duration (10 ms for the input and output spikes) to account for the technological constraints of the memristive elements. Nevertheless, the generality of the demonstration was preserved. Considering the intrinsic deterministic nature of the proposed electronic neuron, spike stimulations were applied at a random time (jitter, with max jitter = 5 ms) within a time window of 50 ms. This approach, combined with a gaussian noise on V_{TH} ($\mu = 0$ V, $\sigma = 0.1$ V), allows the introduction of a variability source to resemble the biological stochastic counterpart. Output spikes were sampled in time windows of 10 ms. To maintain biological realism, the changes in the conductance of the memristors were scaled according to changes of ±50% [from 6 μS (control—CTR) to 9 μS for LTP and from 6 μS to 3 μS for LTD]. This was achieved in circuit simulations by suitably modulating the properties of the memristor via an appropriate choice of the spike shape. Specifically, to accurately simulate the response of the memristor to the stimulation spikes, we employed the UniMORE RRAM model (Fig. 5B), in which the conductance of the device depends on the physical properties of the conductive nanofilament within the device structure, namely, the thickness of the dielectric barrier (x) within the filament. Also, following the analysis in the previous section, each memristor condition (i.e., CTR, LTD, and LTP) is defined for a specific conductance range (related to the barrier window parameter x, internal to the UniMORE RRAM model, with $x \pm 0.2$ nm).

The estimation of MI transfer in control conditions yielded a value of 3.51 bits, which increased to 4.18 bits upon LTP (+19%) and decreased to 2.54 bits (−28%) upon LTD (Fig. 5C). As observed in biological and simulated neurons, changes in MI due to LTP resulted from an anticipation of the first spike (−29.3%) and the reduced variability of the first spike delay

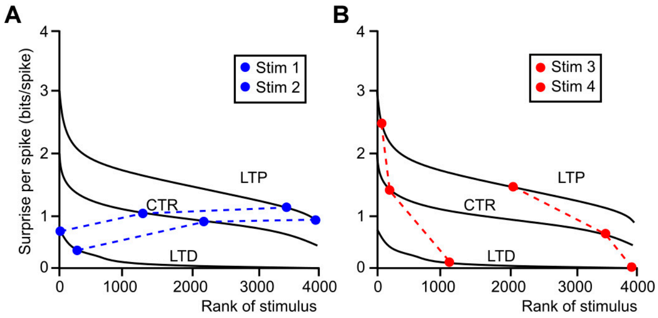

Fig. 6. Surprise per spike (*sps*) as a function of release probability. (A) Black traces show the *sps* values of all 3,876 stimuli for the three different conditions corresponding to low release probability (low conductance/LTD), medium release probability (medium conductance/CTR), and high release probability (high conductance/LTP). Blue circles follow the trend of two different stimuli (1111 1111 1111 1111—stim 1; 1111 1111 1111 0000—stim 2) following changes in memristor conductance. (B) Similar to (A), red circles show changes in two different stimuli with medium and high initial ranks in the low conductance curve (0000 0000 0000 1111—stim3, 0000 0000 0000 0001—stim4).

(−67.1%), coupled with increases in the total number of emitted spikes (17.8%) and the probability of firing (4.6%). The opposite occurred in response to LTD (+92% *sd*; +98% *sj*), where both the firing probability (−11.5%) and the number of emitted spikes (−41.9%) were reduced. These findings show that it is possible to achieve high-fidelity reproductions of biological behaviors during the expression of long-term synaptic plasticity, in terms of both firing characteristics and information transfer, using neuromorphic hardware that mimics actual neuronal microcircuits.

To further confirm the robustness of our estimations, we investigated changes in information transfer induced by long-term plasticity by measuring the surprise per spike in the hardware (see Materials and Methods). This method allows for the highlighting of the contribution of single spikes to the information content by discarding the influence of the firing rate, which has been quantified as approximately 50% of the MI transfer in the simulated MF-GrC synaptic relay [15]. Briefly, the set of MF stimuli was ranked according to the surprise-per-spike value for the three conditions (black traces in Fig. 6), and single stimuli were monitored in their rankings upon changing the memristive conductance that mimicked the expression of LTP and LTD. In qualitative accordance with the simulations (see figure 6 in [15]), stimuli moved within curves following a pattern that increased or decreased their rank depending on their starting positions: stimuli with low initial rankings in the LTD curve tended to increase their positions (Fig. 6A), whereas stimuli with high initial rankings in the LTD curve tended to decrease their positions (Fig. 6B). In all cases, the surprise per spike increased with the increase in release probability. These results confirm the reliability of artificial memristor-based circuits for estimating the information content of specific spike trains.

Discussion

The current study demonstrates that it is possible to transform neurons into electronic circuits that mirror biological actions without losing any important properties. We examined how the abstraction process, initiated with experimental data, can yield hardware architectures that exhibit properties consistent with actual circuits. These findings support recent research showing that neuromorphic microcircuits can exhibit striking biological resemblance [67–69].

Biological versus software and hardware neuromorphic circuits

Neuronal networks serve as the fundamental building blocks of nervous systems across all animal species. From the perspective of generating artificially intelligent systems, the capability of biological circuits to transfer information by conveying trains of action potentials is undoubtedly the most important aspect to consider [70]. In our approach, involving a gradual level of abstraction, we transformed a biological microcircuit into neuromorphic software and, subsequently, into a hardware neural circuit. Although the macroscopic behavior of the system generally remained aligned throughout the simplification phase, a few quantitative deviations were observed. The main factor contributing to these differences is noise. Biological networks are inherently noisy systems [71] given the presence of various stochastic elements involved in the process of neurotransmission ranging from the opening of single ion channels [72] to synaptic vesicle release [73] and post-synaptic receptor activation [74]. To mitigate the intrinsic noise of neuronal circuits, we implemented different strategies at the experimental and simulation levels. First, we limited the sources of variability in MI calculation by focusing on the simplest circuit in the brain: the cerebellar GrC with its afferents [75,76]. Second, synaptic weights were distributed among different afferents while preserving the average weight. Last, long-term plasticity was simulated by changing synaptic strengths in terms of release probability, weights, or memristive conductance. These precautions allowed the in silico reproduction of the experimentally observed biological variability [7,40]. This aspect is particularly important because previous studies have demonstrated that, during long-term plasticity, there is a critical change in the variability of spike generation that can potentially affect the MI transfer [15,16].

At the hardware level, biological circuits have been reproduced by assuming a direct dependency between the release probability and the memristor conductance. Here, we provide evidence that, despite the differences between biological and neuromorphic neurons, complicated computational tasks can be effectively performed by artificial systems [67]. This serves as a proof-of-concept demonstration, showcasing the feasibility of developing electronic neural networks with features comparable to those exhibited by brain circuitry. The idea of reproducing biological performance in hardware has been implemented in the past using different strategies based on materials [77] and/or architectures [78], mimicking the firing of single neurons [66] or the activity of single synapses [79]. Nonetheless, the fundamentals of whether and how hardware circuits are capable of transferring information have never been explored. An important finding of this study is related to the parameters that affect MI estimation the most. It is evident that neuromorphic electronics transfer information by influencing spike timing and firing precision [15,16] (Fig. 4B), rather than by simply modulating the firing frequency and the total number of spikes. Furthermore, we have also shown that, even after discarding the influence of firing rate on information transmission and focusing on single spikes [15], the transferability of biological circuits to artificial networks can be reliably achieved. This evidence supports the robustness of the proposed method for estimating the capability of neuromorphic hardware systems in transferring salient spike-based information. Moreover, different metrics can be adopted to estimate information transfer, such as the correlation among different spike trains [80], frequency dependence coding [18], and incremental MI, which is a measure of network connectivity [81]. The choice of MI allows for reducing the complexity of the observables and, consequently, reducing the size and complexity of neuromorphic hardware. In addition to demonstrating the remarkable capability of neuromorphic hardware to compute sparse and temporally uncorrelated information, these results help pave the way for the development of advanced biorealistic electronic circuits.

The proposed study has been conducted by analyzing one of the crucial issues regarding neuronal function: the manner in which information is transmitted [81–84]. The approach adopted to reproduce in hardware the capabilities of biological circuits required limiting the number of neuronal computational models to be tested. Our hypothesis of circumscribing the number of tests only to (a) morphological [85] and (b) point neuron models [86,87] has been corroborated by results showing that little or no difference can be found during the transition from experiments to hardware. It could be argued that the simplicity of the adopted neuronal class, the cerebellar GrC, with its four inputs, biases the interpretation of the reliability of the process. However, although more complicated neurons with articulated morphologies and multiple inputs would likely lead to error amplification during the conversion process from biological neurons to electronics, the changes in spike-related parameters are comparable [88]. This observation should be respected in different and more articulated network configurations presenting, for instance, highly integrative nodes like hub neurons. This consideration arises from the observation that, although the neuromorphic circuit has not been calibrated and parameterized for specific neuronal behaviors, the first spike delay and variability, which are extremely sensitive to changes in neuronal properties, show similar variations in electronics, simulations, and experiments. Conversely, macroscopic parameters, such as the number of spikes and firing probability, which can both be finely tuned during more sophisticated calibration procedures, show fewer similarities under different testing conditions. Interestingly, these effects on spike-related parameters reverberated in the number of MI changes calculated in the hardware, experiments, and simulations, suggesting similar performance with other network configurations.

Future perspectives and limitations of the study

The demonstration of the biological reliability of neuromorphic circuits is crucial because, unlike conventional hardware, neuromorphic electronics can be designed to operate in a strongly reduced power consumption regime across multiple time domains, accommodating various circuit architectures. This advantage, intrinsically related to the electronic implementation of bioplausible SNNs, will be remarkably useful for several applications in the next few years. In particular, from an electronics standpoint, we expect that the exploration of optimal design strategies for circuits that encode information in the time domain will be crucial. Aspects related to information transfer within such circuits will be coupled with innovative circuit design strategies based on CMOS and innovative devices to target the realization of low-power neuromorphic architectures with a high resemblance to their biological counterparts in terms of information processing, transmission, and energy efficiency. Additionally, from a computational modeling standpoint, further advancements could involve the exploration of different metrics determining information transfer in microcircuits. These metrics may include synchronized and desynchronized firing patterns in neuronal cohorts or the transmitted intersection information, which measures how much of the information content within a neuronal population at a given time is present at a later time in a second population.

These investigations will be fundamental in overcoming some of the limitations of the proposed approach, which include (a) the adoption of the smallest biological circuit, (b) the discard of brain complexity, (c) the use of a single metric (MI) to estimate information transfer, and (d) the choice of time coding over frequency coding to estimate information content. Addressing these aspects may involve increasing the circuit size, adopting additional metrics, and further refining the translation of the remarkable capabilities of brain circuits into biomimetic devices.

Conclusion

In this study, we analyzed information transfer in neuromorphic circuits through a process of abstraction, allowing the conversion of biological neurons into electronic neurons. Importantly, the reduction of biological complexity, typically pursued when abstracting from the real world to a simulation environment, has preserved an essential feature of neuronal circuits: the amount of information transferred during synaptic communication. We believe that this characteristic has been preserved because the information is linked to the timing of spikes rather than their frequency. This evidence could greatly influence the future of neuromorphic computing, given the widely adopted tendency to design devices for frequency-based algorithms.

Acknowledgments

We thank C. Frigeri, technician at the University of Modena and Reggio Emilia, for his valuable technical assistance in maintaining the experimental setup.

Funding: This work has been funded by the following grants: J.M. is supported by the European Union's Horizon 2020 Framework Program for Research and Innovation under the specific GA N°785907 (Human Brain Project SGA2) with a partnering project "SMART-BRAIN" and by the National Recovery and Resilience Plan (NRRP), Mission 4, "Education and Research" Component 2, "From research to Business" Investiment 3.1 – Call for tender No. 3264 of December 28, 2021, of the Italian Ministry of University and Research funded by the European Union—NextGenerationEU—Award Number: Project code IR0000011, Concession Decree No. 117 of June 21, 2022, adopted by the Italian Ministry of University and Research, CUP B51E22000150006, Project title "EBRAINS-Italy (European Brain ReseArch INfrastructureS-Italy)." A.B. and J.M. are supported by the University of Modena and Reggio Emilia with a grant "FAR Dipartimentale 2021." G.M.B. is supported by the Italian Ministry of University and Research (MUR): "Dipartimenti di Eccellenza" Program (2018–2022). D.G. is supported by the Italian Ministry of University and Research (MUR): DM n 1062 del 10/08/2021 PON—"Ricerca e Innovazione 2014–2020," "Azione IV.6 Contratti di ricerca su tematiche Green," and by the University of Modena and Reggio Emilia with a grant "FAR Dipartimentale 2022." T.Z. and F.M.P.

acknowledge partial funding from the National Recovery and Resilience Plan, Mission 04 Component 2 Investment 1.5—NextGenerationEU, Call for Tender No. 3277 dated 30 December 2021, Award Number: 0001052 dated 23 June 2022.

Author contributions: D.G., F.M.P., and J.M. conceived the idea and designed the experiments and simulations. D.G. and J.M. performed electrophysiological recordings. L.B., T.Z., and F.M.P. performed simulations of neuromorphic circuits. D.G. and G.M.B. performed simulations of neuronal models. A.B., F.M.P., and J.M. funded the research. All authors contributed to the writing of the manuscript.

Competing interests: The authors declare that they have no competing interests.

Data Availability

Data and results are available from the corresponding author upon request.

References

1. Testa-Silva G, Verhoog MB, Linaro D, de Kock CP, Baayen JC, Meredith RM, De Zeeuw CI, Giugliano M, Mansvelder HD. High bandwidth synaptic communication and frequency tracking in human neocortex. *PLOS Biol*. 2014;12(11):Article e1002007.
2. Solinas S, Forti L, Cesana E, Mapelli J, De Schutter E, D'Angelo E. Computational reconstruction of pacemaking and intrinsic electroresponsiveness in cerebellar Golgi cells. *Front Cell Neurosci*. 2007;1:2.
3. Solinas S, Forti L, Cesana E, Mapelli J, De Schutter E, D'Angelo E. Fast-reset of pacemaking and theta-frequency resonance patterns in cerebellar golgi cells: Simulations of their impact in vivo. *Front Cell Neurosci*. 2007;1:4.
4. Dobrunz LE, Stevens CF. Heterogeneity of release probability, facilitation, and depletion at central synapses. *Neuron*. 1997;18(6):995–1008.
5. Fassio A, Merlo D, Mapelli J, Menegon A, Corradi A, Mete M, Zappettini S, Bonanno G, Valtorta F, D'Angelo E, et al. The synapsin domain E accelerates the exoendocytotic cycle of synaptic vesicles in cerebellar Purkinje cells. *J Cell Sci*. 2006;119(Pt 20):4257–4268.
6. Petrini EM, Barberis A. Diffusion dynamics of synaptic molecules during inhibitory postsynaptic plasticity. *Front Cell Neurosci*. 2014;8:300.
7. Nieus T, Sola E, Mapelli J, Saftenku E, Rossi P, D'Angelo E. LTP regulates burst initiation and frequency at mossy fiber-granule cell synapses of rat cerebellum: Experimental observations and theoretical predictions. *J Neurophysiol*. 2006;95(2):686–699.
8. Huang YY, Kandel ER. Modulation of both the early and the late phase of mossy fiber LTP by the activation of beta-adrenergic receptors. *Neuron*. 1996;16(3):611–617.
9. Rothman JS, Cathala L, Steuber V, Silver RA. Synaptic depression enables neuronal gain control. *Nature*. 2009;457(7232):1015–1018.
10. Mapelli J, Gandolfi D, D'Angelo E. High-pass filtering and dynamic gain regulation enhance vertical bursts transmission along the mossy fiber pathway of cerebellum. *Front Cell Neurosci*. 2010;4:14.
11. Scanziani M, Malenka RC, Nicoll RA. Role of intercellular interactions in heterosynaptic long-term depression. *Nature*. 1996;380(6573):446–450.
12. Gandolfi D, Bigiani A, Porro CA, Mapelli J. Inhibitory plasticity: From molecules to computation and beyond. *Int J Mol Sci*. 2020;21(5):1805.
13. Krause R, van Bavel JJA, Wu C, Vos MA, Nogaret A, Indiveri G. Robust neuromorphic coupled oscillators for adaptive pacemakers. *Sci Rep*. 2021;11(1):18073.
14. Benatti L, Zanotti T, Gandolfi D, Mapelli D, Puglisi FM. Biologically plausible information propagation in a complementary metal-oxide semiconductor integrate-and-fire artificial neuron circuit with memristive synapses. *Nano Futures*. 2023;7(2):025003.
15. Arleo A, Nieus T, Bezzi M, D'Errico A, D'Angelo E, Coenen OJ-MD. How synaptic release probability shapes neuronal transmission: Information-theoretic analysis in a cerebellar granule cell. *Neural Comput*. 2010;22(8):2031–2058.
16. Mapelli J, Gandolfi D, Giuliani E, Prencipe FP, Pellati F, Barbieri A, D'Angelo E, Bigiani A. The effect of desflurane on neuronal communication at a central synapse. *PLOS ONE*. 2015;10(4):Article e0123534.
17. Ainsworth M, Lee S, Cunningham MO, Traub RD, Kopell NJ, Whittington MA. Rates and rhythms: A synergistic view of frequency and temporal coding in neuronal networks. *Neuron*. 2012;75(4):572–583.
18. Ito HT, Schuman EM. Frequency-dependent signal transmission and modulation by neuromodulators. *Front Neurosci*. 2008;2(2):138–144.
19. Farina D, Negro F, Dideriksen JL. The effective neural drive to muscles is the common synaptic input to motor neurons. *J Physiol*. 2014;592(16):3427–3441.
20. Koay SA, Charles AS, Thiberge SY, Brody CD, Tank DW. Sequential and efficient neural-population coding of complex task information. *Neuron*. 2022;110(2):328–349.e11.
21. Brzosko Z, Mierau SB, Paulsen O. Neuromodulation of spike-timing-dependent plasticity: Past, present, and future. *Neuron*. 2019;103(4):563–581.
22. Ignatov M, Ziegler M, Hansen M, Petraru A, Kohlstedt H. A memristive spiking neuron with firing rate coding. *Front Neurosci*. 2015;9:376.
23. Lanza M, Sebastian A, Lu WD, Le Gallo M, Chang M-F, Akinwande D, Puglisi FM, Alshareef HN, Liu M, Roldan JB. Memristive technologies for data storage, computation, encryption, and radio-frequency communication. *Science*. 2022;376(6597):eabj9979.
24. Florini D, Gandolfi D, Mapelli J, Benatti L, Pavan P, Puglisi FM. A hybrid CMOS-memristor spiking neural network supporting multiple learning rules. *IEEE Trans Neural Netw Learn Syst*. 2022;1–13.
25. Bialek W, Rieke F, de Ruyter van Steveninck RR, Warland D. Reading a neural code. *Science*. 1991;252(5014):1854–1857.
26. Borst A, Theunissen FE. Information theory and neural coding. *Nat Neurosci*. 1999;2(11):947–957.
27. Fuhrmann G, Segev I, Markram H, Tsodyks M. Coding of temporal information by activity-dependent synapses. *J Neurophysiol*. 2002;87(1):140–148.
28. Quian Quiroga R, Panzeri S. Extracting information from neuronal populations: Information theory and decoding approaches. *Nat Rev Neurosci*. 2009;10(3):173–185.
29. Brenner N, Bialek W, de Ruyter van Steveninck R., de Ruyter van Steveninck R. Adaptive rescaling maximizes information transmission. *Neuron*. 2000;26(3):695–702.

30. de Ruyter van Steveninck RR, Lewen GD, Strong SP, Koberle R, Bialek W. Reproducibility and variability in neural spike trains. *Science*. 1997;275(5307):1805–1808.
31. Sharpee TO, Sugihara H, Kurgansky AV, Rebrik SP, Stryker MP, Miller KD. Adaptive filtering enhances information transmission in visual cortex. *Nature*. 2006;439(7079):936–942.
32. Goldman MS. Enhancement of information transmission efficiency by synaptic failures. *Neural Comput*. 2004;16(6):1137–1162.
33. London M, Schreibman A, Häusser M, Larkum ME, Segev I. The information efficacy of a synapse. *Nat Neurosci*. 2002;5(4):332–440.
34. Manwani A, Steinmetz PN, Koch C. The impact of spike timing variability on the signal-encoding performance of neural spiking models. *Neural Comput*. 2002;14(2):347–367.
35. Llinas R, Bloedel JR, Hillman DE. Functional characterization of neuronal circuitry of frog cerebellar cortex. *J Neurophysiol*. 1969;32(6):847–870.
36. D'Angelo E, Mazzarello P, Prestori F, Mapelli J, Solinas S, Lombardo P, Cesana E, Gandolfi D, Congi L. The cerebellar network: From structure to function and dynamics. *Brain Res Rev*. 2011;66(1-2):5–15.
37. Nguyen TM, Thomas LA, Rhoades JL, Ricchi I, Yuan XC, Sheridan A, Hildebrand DGC, Funke J, Regehr WG, Lee W-CA. Structured cerebellar connectivity supports resilient pattern separation. *Nature*. 2023;613(7944):543–549.
38. Mapelli J, Gandolfi D, Giuliani E, Casali S, Congi L, Barbieri A, D'Angelo E, Bigiani A. The effects of the general anesthetic sevoflurane on neurotransmission: An experimental and computational study. *Sci Rep*. 2021;11(1):4335.
39. Mapelli J, Gandolfi D, Vilella A, Zoli M, Bigiani A. Heterosynaptic GABAergic plasticity bidirectionally driven by the activity of pre- and postsynaptic NMDA receptors. *Proc Natl Acad Sci U S A*. 2016;113(35):9898–9903.
40. Mapelli J, Boiani GM, D'Angelo E, Bigiani A, Gandolfi D. Long-term synaptic plasticity tunes the gain of information channels through the cerebellum granular layer. *Biomedicine*. 2022;10(12):3185.
41. Casali S, Tognolina M, Gandolfi D, Mapelli J, D'Angelo E. Cellular-resolution mapping uncovers spatial adaptive filtering at the rat cerebellum input stage. *Commun Biol*. 2020;3(1):635.
42. Krizhevsky A, Sutskever I, Hinton GE. Imagenet classification with deep convolutional neural networks. *Adv Neural Inf Proces Syst*. 2012.
43. Yang S, Tan J, Chen B. Robust spike-based continual meta-learning improved by restricted minimum error entropy criterion. *Entropy*. 2022;24(4):455.
44. Yang S, Linares-Barranco B, Chen B. Heterogeneous ensemble-based spike-driven few-shot online learning. *Front Neurosci*. 2022;16:Article 850932.
45. Yang S, Tan J, Lei T, Linares-Barranco B. Smart traffic navigation system for fault-tolerant edge computing of internet of vehicle in intelligent transportation gateway. *IEEE Trans Intell Transp Syst*. 2023;24(11):13011–13022.
46. Sun B, Guo T, Zhou G, Ranjan S, Jiao Y, Wei L, Zhou YN, Wu YA. Synaptic devices based neuromorphic computing applications in artificial intelligence. *Mater Today Phys*. 2021;18:100393.
47. Yang S, Pang T, Wang H, Lei T, Pan J, Wang J, Jin Y. Spike-driven multi-scale learning with hybrid mechanisms of spiking dendrites. *Neurocomputing*. 2023;542:Article 126240.
48. Malleret G, Alarcon JM, Martel G, Takizawa S, Vronskaya S, Yin D, Chen IZ, Kandel ER, Shumyatsky GP. Bidirectional regulation of hippocampal long-term synaptic plasticity and its influence on opposing forms of memory. *J Neurosci*. 2010;30(10):3813–3825.
49. Gandolfi D, Mapelli J, D'Angelo E. Long-term spatiotemporal reconfiguration of neuronal activity revealed by voltage-sensitive dye imaging in the cerebellar granular layer. *Neural Plast*. 2015;2015:284986.
50. Forti L, Cesana E, Mapelli J, D'Angelo E. Ionic mechanisms of autorhythmic firing in rat cerebellar Golgi cells. *J Physiol*. 2006;574(Pt 3):711–729.
51. Prestori F, Bonardi C, Mapelli L, Lombardo P, Goselink R, De Stefano ME, Gandolfi D, Mapelli J, Bertrand D, Schonewille M, et al. Gating of long-term potentiation by nicotinic acetylcholine receptors at the cerebellum input stage. *PLOS ONE*. 2013;8(5):Article e64828.
52. Sola E, Prestori F, Rossi P, Taglietti V, D'Angelo E. Increased neurotransmitter release during long-term potentiation at mossy fiber-granule cell synapses in rat cerebellum. *J Physiol*. 2004;557(3):843–861.
53. Panzeri S, Senatore R, Montemurro MA, Petersen RS. Correcting for the sampling bias problem in spike train information measures. *J Neurophysiol*. 2007;98(3):1064–1072.
54. Shannon C. The mathematical theory of communication. *Bell Syst Tech J*. 1948;27(3):379–423.
55. Tsodyks MV, Markram H. The neural code between neocortical pyramidal neurons depends on neurotransmitter release probability. *Proc Natl Acad Sci U S A*. 1997;94(2):719–723.
56. Puglisi FM, Zanotti T, Pavan P. Unimore resistive random access memory (RRAM) Verilog-A model. *nanoHUB*. 2019.
57. Campbell KA. Self-directed channel memristor for high temperature operation. *Microelectron J*. 2017;59:10–14.
58. Mapelli J, D'Angelo E. The spatial organization of long-term synaptic plasticity at the input stage of cerebellum. *J Neurosci*. 2007;27(6):1285–1296.
59. D'Angelo E, Solinas S, Mapelli J, Gandolfi D, Mapelli L, Prestori F. The cerebellar Golgi cell and spatiotemporal organization of granular layer activity. *Front Neural Circuits*. 2013;7:93.
60. Gandolfi D, Boiani GM, Bigiani A, Mapelli J. Modeling neurotransmission: Computational tools to investigate neurological disorders. *Int J Mol Sci*. 2021;22(9):4565.
61. D'Angelo E, Solinas S, Garrido J, Casellato C, Pedrocchi A, Mapelli J, Gandolfi D, Prestori F. Realistic modeling of neurons and networks: Towards brain simulation. *Funct Neurol*. 2013;28(3):153–166.
62. Gandolfi D, Mapelli J, Solinas S, De Schepper R, Geminiani A, Casellato C, D'Angelo E, Migliore M. Author correction: A realistic morpho-anatomical connection strategy for modelling full-scale point-neuron microcircuits. *Sci Rep*. 2022;12(1):19792.
63. Gandolfi D, Mapelli J, Solinas SMG, Triebkorn P, D'Angelo E, Jirsa V, Migliore M. Full-scale scaffold model of the human hippocampus CA1 area. *Nat Comput Sci*. 2023;3(3):264–276.
64. Hodgkin AL, Huxley AF. A quantitative description of membrane current and its application to conduction and excitation in nerve. *J Physiol*. 1952;117(4):500–544.
65. Gandolfi D, Cerri S, Mapelli J, Polimeni M, Tritto S, Fuzzati-Armentero M-T, Bigiani A, Blandini F, Mapelli L, D'Angelo E. Activation of the CREB/*c-Fos* pathway during long-term synaptic plasticity in the cerebellum granular layer. *Front Cell Neurosci*. 2017;11:184.

66. Abu-Hassan K, Taylor JD, Morris PG, Donati E, Bortolotto ZA, Indiveri G, Paton JFR, Nogaret A. Optimal solid state neurons. *Nat Commun*. 2019;10(1):5309.
67. Gandolfi D, Puglisi FM, Boiani GM, Pagnoni G, Friston KJ, D'Angelo E, Mapelli J. Emergence of associative learning in a neuromorphic inference network. *J Neural Eng*. 2022;19(3):036022.
68. Bartolozzi C, Indiveri G, Donati E. Embodied neuromorphic intelligence. *Nat Commun*. 2022;13(1):1024.
69. Indiveri G, Linares-Barranco B, Hamilton TJ, van Schaik A, Etienne-Cummings R, Delbruck T, Liu SC, Dudek P, Häfliger P, Renaud S, Schemmel J, Cauwenberghs G, Arthur J, Hynna K, Folowosele F, Saighi S, Serrano-Gotarredona T, Wijekoon J, Wang Y, Boahen K. Neuromorphic silicon neuron circuits. *Front Neurosci*. 2011;5:73.
70. Abbott LF, DePasquale B, Memmesheimer R-M. Building functional networks of spiking model neurons. *Nat Neurosci*. 2016;19(3):350–355.
71. Zylberberg J, Pouget A, Latham PE, Shea-Brown E. Robust information propagation through noisy neural circuits. *PLOS Comput Biol*. 2017;13(4):Article e1005497.
72. Dixon RE, Navedo MF, Binder MD, Santana LF. Mechanisms and physiological implications of cooperative gating of clustered ion channels. *Physiol Rev*. 2022;102(3):1159–1210.
73. Balaji J, Ryan TA. Single-vesicle imaging reveals that synaptic vesicle exocytosis and endocytosis are coupled by a single stochastic mode. *Proc Natl Acad Sci U S A*. 2007;104(51):20576–20581.
74. Ribrault C, Sekimoto K, Triller A. From the stochasticity of molecular processes to the variability of synaptic transmission. *Nat Rev Neurosci*. 2011;12(7):375–387.
75. Mapelli J, Gandolfi D, D'Angelo E. Combinatorial responses controlled by synaptic inhibition in the cerebellum granular layer. *J Neurophysiol*. 2010;103(1):250–261.
76. Jakab RL, Hámori J. Quantitative morphology and synaptology of cerebellar glomeruli in the rat. *Anat Embryol*. 1988;179(1):81–88.
77. Covi E, Brivio S, Serb A, Prodromakis T, Fanciulli M, Spiga S. Analog memristive synapse in spiking networks implementing unsupervised learning. *Front Neurosci*. 2016;10:482.
78. Moro F, Hardy E, Fain B, Dalgaty T, Clémençon P, De Prà A, Esmanhotto E, Castellani N, Blard F, Gardien F, et al. Neuromorphic object localization using resistive memories and ultrasonic transducers. *Nat Commun*. 2022;13(1):3506.
79. Bianchi S, Muñoz-Martin I, Covi E, Bricalli A, Piccolboni G, Regev A, Molas G, Nodin JF, Andrieu F, Ielmini D. A self-adaptive hardware with resistive switching synapses for experience-based neurocomputing. *Nat Commun*. 2023;14(1):1565.
80. Gribkova ED, Ibrahim BA, Llano DA. A novel mutual information estimator to measure spike train correlations in a model thalamocortical network. *J Neurophysiol*. 2018;120(6):2730–2744.
81. Singh A, Lesica NA. Incremental mutual information: A new method for characterizing the strength and dynamics of connections in neuronal circuits. *PLOS Comput Biol*. 2010;6(12):Article e1001035.
82. Singh MS, Pasumarthy R, Vaidya U, Leonhardt S. On quantification and maximization of information transfer in network dynamical systems. *Sci Rep*. 2023;13(1):5588.
83. Roberts TP, Kern FB, Fernando C, Szathmáry E, Husbands P, Philippides AO, Staras K. Encoding temporal regularities and information copying in hippocampal circuits. *Sci Rep*. 2019;9(1):19036.
84. Gandolfi D, Pozzi P, Tognolina M, Chirico G, Mapelli J, D'Angelo E. The spatiotemporal organization of cerebellar network activity resolved by two-photon imaging of multiple single neurons. *Front Cell Neurosci*. 2014;8:92.
85. Cavarretta F, Burton SD, Igarashi KM, Shepherd GM, Hines ML, Migliore M. Parallel odor processing by mitral and middle tufted cells in the olfactory bulb. *Sci Rep*. 2018;8(1):7625.
86. Kobayashi R, Kurita S, Kurth A, Kitano K, Mizuseki K, Diesmann M, Richmond BJ, Shinomoto S. Reconstructing neuronal circuitry from parallel spike trains. *Nat Commun*. 2019;10(1):4468.
87. Muller L, Reynaud A, Chavane F, Destexhe A. The stimulus-evoked population response in visual cortex of awake monkey is a propagating wave. *Nat Commun*. 2014;5:3675.
88. Gandolfi D, Lombardo P, Mapelli J, Solinas S, D'Angelo E. θ-Frequency resonance at the cerebellum input stage improves spike timing on the millisecond time-scale. *Front Neural Circuits*. 2013;7:64.